REPORT DOCUMENTATION PA

AFRL-SR-BL-TR-02-

00255

roved

)4-0188

Public reporting for this collection of information is estimated to average 1 hour per response, including maintaining the data needed, and completing and reviewing the collection of information. Send comment including suggestions for reducing this burden, to Washington Headquarters Services, Directorate for ... gathering and ...n of information, ... Reports, 1215 Jefferson Davis Highway, Suite 1204, Arlington, VA 22202-4302, and to the Office of Management and Budget, Paperwork Reduction Project (0704-0188), Washington, DC 20503.

1. AGENCY USE ONLY (Leave Blank)	2. REPORT DATE	3. REPORT TYPE AND DATES COVERED
	20 DEC 0l	Final Technical 1 Aug 98 – 31 Aug 00

4. TITLE AND SUBTITLE

Fast Methods for Electromagnetic Modeling of Complex Geometries

5. FUNDING NUMBERS

F49620-98-C-0035

6. AUTHOR(S)

J. J. Ottusch, G. D. Simms, J. L. Visher, S. M. Wandzura

7. PERFORMING ORGANIZATION NAME(S) AND ADDRESS(ES)

HRL Laboratories, LLC
3011 Malibu Canyon Road
Malibu, CA 90265

8. PERFORMING ORGANIZATION REPORT NUMBER

9. SPONSORING/MONITORING AGENCY NAME(S) AND ADDRESS(ES)

Air Force Office of Scientific Research
801 North Randolph Street, Room 732
Arlington, VA 22203-1977

10. SPONSORING/MONITORING AGENCY REPORT NUMBER

11. SUPPLEMENTARY NOTES

AIR FORCE OFFICE OF SCIENTIFIC RESEARCH (AFOSR)
NOTICE OF TRANSMITTAL DTIC. THIS TECHNICAL REPORT
HAS BEEN REVIEWED AND IS APPROVED FOR PUBLIC RELEASE
LAW AFR 190-12. DISTRIBUTION IS UNLIMITED.

12a. DISTRIBUTION/AVAILABILITY STATEMENT

Distribution Statement A. Approved for public release; distribution is unlimited.

12b. DISTRIBUTION CODE

13. ABSTRACT (maximum 200 words)

This report describes several areas of research that address areas that are important for practical use of modern techniques of computational electromagn... ics, with emphasis on methods that, my making code more robust, will reduce the need for human attention. This include low frequency fast multipole methods, appr... ate discretization to efficiently model charge and current distribution near geometric singularities, new, more efficient quadrature rules, and a system to auto... ate the patch refinement process.

20020118 099

14. SUBJECT TERMS

15. NUMBER OF PAGES

34

16. PRICE CODE

17. SECURITY CLASSIFICATION OF REPORT	18. SECURITY CLASSIFICATION OF THIS PAGE	19. SECURITY CLASSIFICATION OF ABSTRACT	20. LIMITATION OF ABSTRACT
Unclassified	Unclassified	Unclassified	UL

HRL REF 80036

Fast Methods for Electromagnetic Modeling of Complex Geometries

Final Technical Report

December 2001

J. J. Ottusch G. D. Simms J. L. Visher S. M. Wandzura

Computational Physics Department
Information Sciences Laboratory
HRL Laboratories, LLC

Principal Investigator and Program Manager

Stephen Wandzura
310/317-5462
wandzura@hrl.com

Air Force Office of Scientific Research
Contract #F49620-98-C-0035

Sponsored by
Defense Advanced Research Projects Agency
Defense Sciences Office

Approved for public release; distribution is unlimited.

Contents

Chapter 1

Edge Constraints

We have developed discretizations that capture the singular behavior of currents on open edges in a high-order manner. These discretizations use the analytic properties of currents along infinity long, open edges. Consider the metallization that covers the half plane $x > 0$. The current normal to the edge at $x = 0$, $\sim x^{1/2+q}, q \in [0 \ldots)$, and the current transverse to the same edge is proportional to $x^{-1/2+q}$. The appropriate testing functions and quadratures are the Gauss-Jacobi polynomials and quadratures. All experiments indicate that this is a very good method, where the number of points/wavelength to achieve a given accuracy is of the order of what is need for regular discretizations of regular geometries. The constraint that currents don't go off the edge is implicit in the discretization of the integral equations.

The singular behavior of current along creases is much more complex. However, the current along the edge is infinite, with leading singularity proportional to $x^{\pi/\phi-1}$ where ϕ is the angle of the bend, while the current across the crease is finite. It is only very special geometries with special excitations that the error in the current across the edge dominates. The way we have chosen to capture the singular current along the edge is to increase the density of discretization points by tapering patches. When the large currents along the edge have been resolved to the desired accuracy, the currents across the crease are captured even more accurately.

This characterization of the current along geometric singularities is confirmed with experiments using the automatic patch refinement code developed as part of the contract. To be specific, it is seen that along the edges of a cube, the patches must be tapered towards the edge to resolve the current along the edge, and this current is orders of magnitude larger than the

current flowing across the edge.

The singular discretizations have been applied to rectangles, sharp elbows, tee structures, cross structures and PECs separated by gaps of width $\lambda/50$, all with good results. Care must be taken when applying the method to sharp corners to ensure the singular currents are represented with the discretization.

Below are tables from the simplest geometry studied – a $3\lambda \times 4\lambda$ PEC rectangle with zero thickness. The solution used for comparison is the 12th order singular discretization. Using the singular discretization with 10 points per wavelength, the error is $1.3 \cdot 10^{-3}$; this compares well with the accuracy obtained with a regular discretization of a regular geometry using the EFIE and 10 points per wavelength. The second table demonstrates the performance of a first order discretization of the same rectangle.

Order	Points	Points/λ	Error
2	48	2	4.4
4	192	4	$8.6 \cdot 10^{-1}$
6	432	6	$6.1 \cdot 10^{-2}$
8	768	8	$5.6 \cdot 10^{-3}$
10	1200	10	$1.3 \cdot 10^{-3}$

Table 1.1: RMS error of Gauss-Jacobi method on $3\lambda \times 4\lambda$ rectangle.

Points	Points/λ	Error
1200	10	$9.9 \cdot 10^{-1}$
4800	20	$3.1 \cdot 10^{-1}$
7500	25	$2.5 \cdot 10^{-1}$

Table 1.2: RMS error of first order method with uniform mesh on $3\lambda \times 4\lambda$ rectangle.

Chapter 2

Wave Quadratures

2.1 Theory

The idea is that in integrating oscillatory functions, one can do better than Gaussian quadrature. The prescription is to use formula that give accurate results for some spectrum of waves, rather than a finite set of polynomials. We first illustrate how this can be done on an interval.

2.1.1 Quadrature on a Line

The prescription is to pick weights (or "charges") w_n and abscissae (or "positions") x_n so as to minimize

$$\begin{aligned} E(x,w;\sigma) &\equiv \int d\mu\,\omega(\mu)\left|\sum_n w_n e^{i\mu x_n} - \frac{1}{2}\int_{-1}^{1} dx\, e^{i\mu x}\right|^2 \\ &= \int d\mu\,\omega(\mu)\left|\sum_n w_n e^{i\mu x_n} - \frac{\sin(\mu)}{\mu}\right|^2 \\ &= W(\sigma) + \sum_n w_n V(x_n;\sigma) + \sum_{n,n'} w_n w_{n'} U(x_n - x_{n'};\sigma)\,, \end{aligned} \tag{2.1}$$

where σ is a parameter of the spectrum $\omega(\mu)$, and

$$\begin{aligned} W(\sigma) &= \int d\mu\,\omega(\mu;\sigma)\left(\frac{\sin\mu}{\mu}\right)^2 = \frac{1}{4}\int_{-1}^{1} dx\, V(x;\sigma) \qquad (2.2) \\ V(x;\sigma) &= -2\int d\mu\,\omega(\mu;\sigma)\cos\mu x\frac{\sin\mu}{\mu} \end{aligned}$$

$$= -\int_{-1}^{1} dx'\, U(x-x';\sigma) \tag{2.3}$$

$$U(x-x';\sigma) = \int d\mu\, \omega(\mu;\sigma) e^{i\mu(x-x')}\,. \tag{2.4}$$

We see the problem is equivalent to finding a minimum energy configuration of particles with charges w_n in an external potential $V(x_n)$ and interacting with a potential $U(x_n - x_{n'})$. Another possible choice is a top-hat spectrum,

$$\omega(\mu) = \Theta(\sigma^2 - \mu^2)\,, \tag{2.5}$$

however, we chose to simplify the integrals by studying the case of a Gaussian spectrum.

Gaussian Spectrum

If we choose

$$\omega(\mu) = \frac{1}{\sqrt{\pi}\sigma} e^{-\mu^2/\sigma^2}\,, \tag{2.6}$$

then

$$W = \frac{1}{\sigma}\left(\frac{e^{-\sigma^2}-1}{\sigma} + \sqrt{\pi}\,\mathrm{erf}\,\sigma\right) \tag{2.7}$$

$$V(x) = \frac{-\sqrt{\pi}}{\sigma}\left(\mathrm{erf}\,\frac{\sigma(1+x)}{2} + \mathrm{erf}\,\frac{\sigma(1-x)}{2}\right) \tag{2.8}$$

$$U(x-x') = e^{-\frac{\sigma^2}{4}(x-x')^2}\,. \tag{2.9}$$

Small σ limit If one expands E in a power series in σ^2, one finds that the minimization of the successive term in the series enforce the conditions

$$\sum_m w_m x_m^n = \frac{1}{2}\int_{-1}^{1} dx\, x^n\,, \tag{2.10}$$

so that the small σ limit reproduces Gauss-Legendre quadrature, as should be expected.

Large σ limit In this limit, the one-particle potential V becomes very flat except near the endpoints. The two-particle potential repels the points to equal spacing, so that the abscissae become equally spaced.

Fast evaluation of $V(x)$ Although we have a closed form for $V(x)$, in more complicated cases (e.g. triangles), this is not the case. In such cases, a fast evaluation method may be used to make the derivation of quadrature rules more efficient. The one-particle potential is proportional to a convolution of of the two-particle potential with the domain of integration:

$$-V(x;\sigma) = \int_{-1}^{1} dx' \, e^{-\frac{\sigma^2(x-x')^2}{4}} \tag{2.11}$$

$$= \frac{2}{\sigma} \int_{-\sigma/2}^{\sigma/2} d\xi \, e^{-(\sigma x/2-\xi)^2} . \tag{2.12}$$

By using the generating function for the Hermite polynomials[AW95], we can write this as a power series about the point $2x = \xi_0/\sigma$:

$$-V(x;\sigma) = \frac{2}{\sigma} \sum_{m=0}^{\infty} c_m(\xi_0,\sigma) \, (\sigma x/2 - \xi_0)^m \, , \tag{2.13}$$

where

$$c_m(\xi_0,\sigma) \equiv \frac{1}{m!} \int_{-\sigma/2}^{\sigma/2} d\xi \, h_m(\xi - \xi_0) \tag{2.14}$$

$$= \frac{1}{m!} \left[h_{m-1}(-\sigma/2 - \xi_0) - h_{m-1}(\sigma/2 - \xi_0) \right] , \tag{2.15}$$

$$h_{-1}(\xi) \equiv -\frac{\sqrt{\pi}}{2} \operatorname{erf}(\xi) \tag{2.16}$$

$$h_m(\xi) \equiv e^{-\xi^2} H_m(\xi) \quad ; \quad m \geq 0 \tag{2.17}$$

and the H_m are Hermite polynomials. In more general cases the closed form for the coefficients will not be available. In any case, they will be evaluated for a dense enough set of ξ_0 (these are FMM group centers) that the power series will converge reasonably rapidly. In particular if we let

$$\xi_0 \to \xi_n = \frac{\sigma}{2} \frac{2n-1-N}{N} \quad ; \quad n = 1, \ldots, N \, , \tag{2.18}$$

with

$$N = \lceil \sigma \rceil \, , \tag{2.19}$$

then

$$\left| \frac{\sigma x}{2} - \xi_n \right| \leq \frac{1}{2} , \tag{2.20}$$

if we choose $n = \lceil N(x+1)/2 \rceil$ (or 1, if $x = -1$). (The smallest integer not less than x is denoted by $\lceil x \rceil$. The power series may be truncated at a value of m equal to the number of digits of precision desired. For $\sigma \gg 1$, direct evaluation of the integrals for the coefficients $c_m(\xi_n)$ becomes expensive. To deal with this, we again use the Hermite generating function to write

$$c_m(\xi_0, \sigma) = \frac{1}{m!} \int_{-\sigma/2}^{\sigma/2} d\xi \, h_m(\xi - \xi_0) \tag{2.21}$$

$$= \frac{1}{m!} \sum_{n=1}^{N} \int_{\xi_n - \frac{\sigma}{2N}}^{\xi_n + \frac{\sigma}{2N}} d\xi \, h_m(\xi - \xi_0) \,. \tag{2.22}$$

We then use the identity

$$h_m(\xi - \xi_0) = \sum_{l=0}^{\infty} \frac{(\xi_n - \xi)^l}{l!} h_{m+l}(\xi_n - \xi_0) \tag{2.23}$$

to get

$$c_m(\xi_0, \sigma) = \frac{1}{m!} \sum_{n=1}^{N} \sum_{l=0}^{\infty} d_{nl} h_{m+l}(\xi_n - \xi_0) \,, \tag{2.24}$$

where

$$d_{nl} = \frac{1}{l!} \int_{\xi_n - \frac{\sigma}{2N}}^{\xi_n + \frac{\sigma}{2N}} (\xi_n - \xi)^l \tag{2.25}$$

$$= \frac{2}{(l+1)!} \left(\frac{\sigma}{2N} \right)^{l+1} . \tag{2.26}$$

The last equality is one for which we have hope of analytic evaluation in more general cases. Note that the d_{nl} are independent of ξ_0, which is what makes this method "fast". The sum over l may also be truncated at the number of digits of precisions desired.

Numerical Minimization

For now, work directly with the xs and ws. Depending on the minimization method used, we may require up to second derivatives of E with respect to the parameters. These are given by

$$\frac{\partial E}{\partial w_n} = V(x_n) + 2 \sum_{n'} w_{n'} U(x_n - x_{n'}) \tag{2.27}$$

$$\frac{\partial E}{\partial x_n} = w_n V'(x_n) + 2w_n \sum_{n'} w_{n'} U'(x_n - x_{n'}) \tag{2.28}$$

$$\frac{\partial^2 E}{\partial w_n \partial w_{n'}} = 2U'(x_n - x_{n'}) \tag{2.29}$$

$$\frac{\partial^2 E}{\partial w_n \partial x_{n'}} = \delta_{nn'} V'(x_n) - 2w_{n'} U'(x_n - x_{n'}) + 2\delta_{nn'} \sum_{n''} w_{n''} U'(x_n - x_{n''}) \tag{2.30}$$

$$\frac{\partial^2 E}{\partial x_n \partial x_{n'}} = w_n \delta_{nn'} V''(x_n) + 2\delta_{nn'} w_n \sum_{n''} w_{n''} U''(x_n - x_{n''}) - 2w_n w_{n'} U''(x_n - x_{n'}) \,. \tag{2.31}$$

Since the energy is quadratic in the weights, they can be eliminated using $\partial E/\partial w_n = 0$. Letting $\bar{E}(x)$ denote the minimum of $E(x, w)$, with respect to the ws, we have

$$\bar{E} = W - \frac{1}{4} \sum_{nn'} V_n U^{-1}_{nn'} V_{n'} \tag{2.32}$$

$$\frac{\partial \bar{E}}{\partial x_n} = -\frac{1}{2} V'_n \sum_{n'} U^{-1}_{nn'} V_{n'} + \frac{1}{2} V_n \sum_{ll'n'} U^{-1}_{nl} U'_{ll'} U^{-1}_{l'n'} V_{n'} \,, \tag{2.33}$$

where

$$V_n \equiv V(x_n) \tag{2.34}$$

$$V'_n \equiv V'(x_n) \tag{2.35}$$

$$U_{nn'} \equiv U(x_n - x'_n) \tag{2.36}$$

$$U'_{nn'} \equiv U'(x_n - x'_n) \tag{2.37}$$

$$\sum_l U_{nl} U^{-1}_{ln'} = \delta_{nn'} \,. \tag{2.38}$$

Note that U' is antisymmetric.

2.1.2 Quadrature on Symmetric Regions

We classify sets of group-equivalent points in d dimensions and parameterize their coordinates, $\mathbf{x} = \{x_1, \ldots, x_i, \ldots, x_d\}$. There are many different types of indices in the notation and it takes some care to keep them

straight. We take A sets of abscissae labeled by α, parameterized by $\{\lambda_\alpha\} = \lambda_{\alpha 1}, \ldots, \lambda_{\alpha\kappa}, \ldots, \lambda_{i\mu_\alpha}$ (μ_α may vanish), having multiplicity M_α, each associated with a weight w_α. (In the cases we have done so far, $d = 2$, so $0 \leq \mu_i \leq 2$.) Thus for each λ_α, there are functions $x_{li}(\lambda_\alpha)$ for $l = 1, \ldots, M_\alpha$ and $i = 1, \ldots, d$. The energy function to be minimized is then

$$\begin{aligned} E &= W(\sigma) + \sum_{\alpha=1}^{A} w_\alpha M_\alpha V\left[\mathbf{x}_1\left(\lambda_\alpha\right); \sigma\right] \\ &\quad + \sum_{\alpha=1}^{A} w_\alpha M_\alpha \sum_{\beta=1}^{A} \sum_{l=1}^{M_\beta} w_\beta U\left[\mathbf{x}_1\left(\lambda_\alpha\right) - \mathbf{x}_l\left(\lambda_\beta\right); \sigma\right] . \end{aligned} \tag{2.39}$$

[If we need to, we could assume a rotationally symmetric spectrum, so that $V(\mathbf{x}) = V(x)$ and $U(\mathbf{x}) = U(x)$.] Minimizing with respect to w_α, we have

$$\begin{aligned} 0 &= M_\alpha V\left[\mathbf{x}_1\left(\lambda_\alpha\right); \sigma\right] + M_\alpha \sum_{\beta=1}^{A} \sum_{l=1}^{M_\beta} w_\beta U\left[\mathbf{x}_1\left(\lambda_\alpha\right) - \mathbf{x}_l\left(\lambda_\beta\right); \sigma\right] \\ &\quad + \sum_{\beta=1}^{A} w_\beta M_\beta \sum_{l=1}^{M_\alpha} U\left[\mathbf{x}_1\left(\lambda_\beta\right) - \mathbf{x}_l\left(\lambda_\alpha\right); \sigma\right] \end{aligned} \tag{2.40}$$

Because U is an even function, this is a symmetric system of equations. In fact, the two terms in the U are equal because the symmetry of the integration is also a symmetry of U. This can be simplified if we define

$$\bar{U}\left(\lambda_\alpha, \lambda_\beta; \sigma\right) \equiv M_\alpha \sum_{l=1}^{M_\beta} U\left[\mathbf{x}_1\left(\lambda_\alpha\right) - \mathbf{x}_l\left(\lambda_\beta\right); \sigma\right] = \bar{U}_{\alpha\beta} = \bar{U}_{\beta\alpha} \tag{2.41}$$

$$\bar{V}\left(\lambda_\alpha; \sigma\right) \equiv M_\alpha V\left[\mathbf{x}_1\left(\lambda_\alpha\right); \sigma\right] = \bar{V}_\alpha . \tag{2.42}$$

Then

$$E = W + \sum_{\alpha=1}^{A} w_\alpha \bar{V}_\alpha + \sum_{\alpha,\beta=1}^{A} w_\alpha \bar{U}_{\alpha\beta} w_\beta . \tag{2.43}$$

As before, we can either treat the weights as independent variables or eliminate them.

Independent weights

If we consider the weights and abscissae as independent, useful partial derivatives are

$$\frac{\partial E}{\partial w_\alpha} = \bar{V}_\alpha + 2 \sum_{\beta=1}^{A} \bar{U}_{\alpha\beta} w_\beta \tag{2.44}$$

$$\frac{\partial E}{\partial \lambda_{\alpha\kappa}} = w_\alpha \bar{V}'_{\alpha\kappa} + 2w_\alpha \sum_{\beta=1}^{A} \bar{U}'_{\alpha\kappa\beta} w_\beta \tag{2.45}$$

$$\frac{\partial^2 E}{\partial w_\alpha \partial w_\beta} = 2\bar{U}_{\alpha\beta} \tag{2.46}$$

$$\frac{\partial^2 E}{\partial w_\alpha \partial \lambda_{\beta\kappa}} = \delta_{\alpha\beta} \bar{V}'_{\beta\kappa} - 2w_\beta \bar{U}'_{\alpha\kappa\beta} + 2\delta_{\alpha\beta} \sum_{\beta'=1}^{A} \bar{U}_{\alpha\kappa\beta'} \tag{2.47}$$

$$\begin{aligned} \frac{\partial^2 E}{\partial \lambda_{\alpha\kappa} \partial \lambda_{\beta\nu}} &= \delta_{\alpha\beta} w_\alpha w_\beta \bar{V}''_{\alpha\kappa\nu} + 2\delta_{\alpha\beta} w_\alpha \sum_{\beta'=1}^{A} \bar{U}^{(2a)}_{\alpha\kappa\nu\beta'} w_{\beta'} \\ &\quad -2w_\alpha w_\beta \bar{U}^{(2b)}_{\alpha\kappa\beta\nu}, \end{aligned} \tag{2.48}$$

where

$$\bar{V}'_{\alpha\kappa} \equiv \frac{\partial \bar{V}_\alpha}{\partial \lambda_{\alpha\kappa}} = M_\alpha \sum_{i=1}^{d} \frac{\partial x_{1i}(\lambda_\alpha)}{\partial \lambda_{\alpha\kappa}} V_i \left[\mathbf{x}_1(\lambda_\alpha); \sigma\right] \tag{2.49}$$

$$\begin{aligned} \bar{U}'_{\alpha\kappa\beta} &\equiv \frac{\partial \bar{U}(\lambda_\alpha, \lambda_\beta)}{\partial \lambda_{\alpha\kappa}} \\ &= M_\alpha \sum_{l=1}^{M_\beta} \sum_{i=1}^{d} \frac{\partial x_{1i}(\lambda_\alpha)}{\partial \lambda_{\alpha\kappa}} U_i \left[\mathbf{x}_1(\lambda_\alpha) - \mathbf{x}_l(\lambda_\beta)\right] \end{aligned} \tag{2.50}$$

$$\begin{aligned} \bar{V}''_{\alpha\kappa\nu} &\equiv \frac{\partial \bar{V}'_{\alpha\kappa}}{\partial \lambda_{\alpha\nu}} \\ &= M_\alpha \sum_{i=1}^{d} \frac{\partial^2 x_{1i}}{\partial \lambda_{\alpha\kappa} \partial \lambda_{\alpha\nu}} V_i[\mathbf{x}_1(\lambda_\alpha)] \\ &\quad + M_\alpha \sum_{i,j=1}^{d} \frac{\partial x_{1i}(\lambda_\alpha)}{\partial \lambda_{\alpha\kappa}} \frac{\partial x_{1j}(\lambda_\alpha)}{\partial \lambda_{\alpha\nu}} V_{ij}[\mathbf{x}_1(\lambda_\alpha)] \end{aligned} \tag{2.51}$$

$$\begin{aligned} \bar{U}^{(2a)}_{\alpha\kappa\nu\gamma} &\equiv M_\alpha \sum_{l=1}^{M_\gamma} \sum_{i=1}^{d} \Big\{ \frac{\partial^2 x_{1i}}{\partial \lambda_{\alpha\kappa} \partial \lambda_{\alpha\nu}} U_i \left[\mathbf{x}_1(\lambda_\alpha) - \mathbf{x}_l(\lambda_\gamma)\right] \\ &\quad + \frac{\partial x_{1i}(\lambda_\alpha)}{\partial \lambda_{\alpha\kappa}} \sum_{j=1}^{d} \frac{\partial x_{1j}(\lambda_\alpha)}{\partial \lambda_{\alpha\nu}} U_{ij} \left[\mathbf{x}_1(\lambda_\alpha) - \mathbf{x}_l(\lambda_\gamma)\right] \Big\} \end{aligned} \tag{2.52}$$

$$\bar{U}^{(2b)}_{\alpha\kappa\beta\nu} \equiv M_\alpha \sum_{l=1}^{M_\beta} \sum_{i,j=1}^{d} \frac{\partial x_{1i}(\lambda_\alpha)}{\partial \lambda_{\alpha\kappa}} \frac{\partial x_{li}(\lambda_\beta)}{\partial \lambda_{\beta\nu}} U_{ij} \left[\mathbf{x}_1(\lambda_\alpha) - \mathbf{x}_l(\lambda_\beta)\right] \tag{2.53}$$

$$V_i[\mathbf{x}] \equiv \frac{\partial V(\mathbf{x})}{\partial x_i} \tag{2.54}$$

$$U_i[\mathbf{x}] \equiv \frac{\partial U(\mathbf{x})}{\partial x_i} \tag{2.55}$$

$$V_{ij}[\mathbf{x}] \equiv \frac{\partial}{\partial x_j} V_i[\mathbf{x}] \tag{2.56}$$

$$U_{ij}[\mathbf{x}] \equiv \frac{\partial}{\partial x_j} U_i[\mathbf{x}]\,. \tag{2.57}$$

Dependent weights

If we eliminate the weights by minimizing, we have

$$\bar{w}_\alpha\left(\{\lambda\}\right) = -\frac{1}{2}\sum_{\beta=1}^{A} \bar{U}^{-1}_{\alpha\beta}\left(\{\lambda\}\right)\bar{V}_\beta\,. \tag{2.58}$$

It is important to remember that while $\bar{U}_{\alpha\beta}$ is a function of λ_α and λ_β only, $\bar{U}^{-1}_{\alpha\beta}$ is a function of *all* λ. We then have

$$\begin{aligned}
\bar{E}\left(\{\lambda\}\right) &= W - \frac{1}{4}\sum_{\alpha,\beta=1}^{A} \bar{V}_\alpha \bar{U}^{-1}_{\alpha\beta}\bar{V}_\beta \\
&= W + \frac{1}{2}\sum_{\alpha=1}^{A} \bar{w}_\alpha \bar{V}_\alpha \qquad (2.59) \\
\frac{\partial \bar{E}}{\partial \lambda_{\alpha\kappa}} &= -\frac{1}{2}\bar{V}'_{\alpha\kappa}\sum_\beta \bar{U}^{-1}_{\alpha\beta}\bar{V}_\beta + \frac{1}{2}\sum_{\alpha,\alpha',\beta=1}^{A} \bar{V}_\alpha \bar{U}^{-1}_{\alpha\gamma}\bar{U}'_{\gamma\kappa\alpha'}\bar{U}^{-1}_{\alpha'\beta}\bar{V}_\beta \\
&= \bar{V}'_{\alpha\kappa}\bar{w}_\alpha + 2\bar{w}_\alpha\sum_{\beta=1}^{A}\bar{U}'_{\alpha\kappa\beta}\bar{w}_\beta\,, \qquad (2.60)
\end{aligned}$$

2.1.3 Quadrature on a Triangle

The quadrature rule we want approximates integrals over a triangle, with vertices chosen conventionally to be

$$\mathbf{v}_1 = (1,0) \tag{2.61}$$

$$\mathbf{v}_2 = (-1/2, \sqrt{3}/2) \tag{2.62}$$

$$\mathbf{v}_2 = (-1/2, -\sqrt{3}/2)\,. \tag{2.63}$$

Then the integral we are trying to approximate is

$$\frac{1}{A}\int_\triangle d^2\mathbf{x}\, e^{-i\mathbf{q}\cdot\mathbf{x}} = \frac{1}{s_1 s_2}e^{i(s_1-s_2)/3} + \frac{1}{s_2 s_3}e^{i(s_2-s_3)/3} + \frac{1}{s_3 s_1}e^{i(s_3-s_1)/3}\,, \tag{2.64}$$

where

$$A \equiv \frac{3^{3/2}}{4} \tag{2.65}$$

$$s_1 \equiv \mathbf{q}\cdot(\mathbf{v}_2-\mathbf{v}_3) \tag{2.66}$$

$$s_2 \equiv \mathbf{q}\cdot(\mathbf{v}_3-\mathbf{v}_1) \tag{2.67}$$

$$s_3 \equiv \mathbf{q}\cdot(\mathbf{v}_1-\mathbf{v}_2)\,. \tag{2.68}$$

Gaussian Spectrum

The one body potential is

$$V(\mathbf{x};\sigma) = -\frac{2}{A}\int_{\triangle} d^2\mathbf{x}'\, U(\mathbf{x}-\mathbf{x}') \tag{2.69}$$

where the two body potential is

$$U(\mathbf{x};\sigma) = e^{-\frac{\sigma^2}{4}x^2}\,. \tag{2.70}$$

Evaluation of $V(x)$ We have not be able to find a closed form for the single-particle potential, but can reduce it to one numerical integration (actually six integrations). This may be sufficiently fast that one won't have to take the trouble to do it *really* fast. The first step is to change the integral over the triangle $\triangle$ to an integral over its boundary $\partial\triangle$. Note that we can write the two body potential as

$$U(\mathbf{x}) = \nabla^2 Y(\mathbf{x}) \tag{2.71}$$

where

$$Y(\mathbf{x};\sigma) \equiv \frac{1}{\sigma^2}\left[E_1\left(\frac{\sigma^2x^2}{4}\right)+\log\left(\frac{\sigma^2x^2}{4}\right)\right]\,. \tag{2.72}$$

Then using Gauss' theorem,

$$V(\mathbf{x};\sigma) = -\frac{2}{A}\int_{\partial\triangle} dx'\hat{n}\cdot\nabla Y(\mathbf{x}-\mathbf{x}')\,. \tag{2.73}$$

Consider for the moment the contribution of the integral over one side (side three, say, connecting $\mathbf{v}_1$ and $\mathbf{v}_2$) of the triangle to this potential. With a

suitable definition of h, l_1, and l_2, this is

$$
\begin{aligned}
V_3(\mathbf{x}) &= -\frac{2}{A}\frac{\partial}{\partial h}\int_0^{l_1} dx\, Y\left(\sqrt{x^2+h^2};\sigma\right) + [l_1 \to l_2] && (2.74)\\
&= -\frac{2}{A}\frac{2h}{\sigma^2}\int_0^{l_1} dx\, \frac{1-\exp\left[-\frac{\sigma^2}{4}(h^2+x^2)\right]}{h^2+x^2} + [l_1 \to l_2] && (2.75)\\
&= -\frac{2}{A}\frac{2h}{\sigma^2}\int_0^{\sigma^2/4} d\lambda \int_0^{l_1} dx\, e^{-\lambda(h^2+x^2)} + [l_1 \to l_2] && (2.76)\\
&= -\frac{2}{A}\frac{\sqrt{\pi}h}{\sigma^2}\int_0^{\sigma^2/4} d\lambda\, \frac{e^{-\lambda h^2}\,\mathrm{erf}\left(\sqrt{\lambda}l_1\right)}{\sqrt{\lambda}} + [l_1 \to l_2] && (2.77)\\
&= -\frac{2}{A}\left[\frac{\pi}{\sigma^2}\,\mathrm{erf}\,\frac{\sigma l_1}{2}\,\mathrm{erf}\,\frac{\sigma h}{2}\right.\\
&\qquad \left. -\frac{\sqrt{\pi}l_1}{\sigma^2}\int_0^{\sigma^2/4} d\lambda\, \frac{e^{-\lambda l_1^2}\,\mathrm{erf}\left(\sqrt{\lambda}h\right)}{\sqrt{\lambda}}\right] + [l_1 \to l_2] && (2.78)\\
&= -\frac{2}{A}\frac{2}{\sigma^2}\nu\left(\frac{\sigma h}{2},\frac{\sigma l_1}{2}\right) + [l_1 \to l_2]\,, && (2.79)
\end{aligned}
$$

where

$$
\begin{aligned}
\nu(\eta,\xi) &\equiv \eta\int_0^{\xi} d\zeta \frac{1-e^{-\eta^2-\zeta^2}}{\eta^2+\zeta^2} && (2.80)\\
&= \frac{\sqrt{\pi}}{2}\eta\int_0^1 d\lambda\, \frac{e^{-\lambda\eta^2}\,\mathrm{erf}\,\sqrt{\lambda}\xi}{\sqrt{\lambda}} && (2.81)\\
&= \frac{\pi}{2}\,\mathrm{erf}\,\eta\,\mathrm{erf}\,\xi - \frac{\sqrt{\pi}}{2}\xi\int_0^1 d\lambda\, \frac{e^{-\lambda\xi^2}\,\mathrm{erf}\,\sqrt{\lambda}\eta}{\sqrt{\lambda}}\,. && (2.82)
\end{aligned}
$$

We expect the second expression to be more useful for $\eta > \xi$ and the last for $\xi > \eta$.

The suitable definitions are

$$
\begin{aligned}
l_1 &= \frac{(\mathbf{x}-\mathbf{v}_1)\cdot(\mathbf{v}_2-\mathbf{v}_1)}{|\mathbf{v}_1-\mathbf{v}_2|} = \frac{1}{\sqrt{3}}\left[(\mathbf{x}-\mathbf{v}_1)\cdot(\mathbf{v}_2-\mathbf{v}_1)\right] && (2.83)\\
l_2 &= \frac{(\mathbf{x}-\mathbf{v}_2)\cdot(\mathbf{v}_1-\mathbf{v}_2)}{|\mathbf{v}_1-\mathbf{v}_2|} = |\mathbf{v}_1-\mathbf{v}_2| - l_1 && (2.84)\\
h &= \sqrt{(\mathbf{x}-\mathbf{v}_1)^2 - l_1^2}\,. && (2.85)
\end{aligned}
$$

2.2 Numerical Results

In addition to the Gauss–Legendre rule, we have implemented two new quadrature rules in the FastScat program. The first is optimized to approximate the integral of functions containing a flat spectrum of wavenumbers on a triangular patch, up to a cutoff. The second is optimized for a Gaussian spectrum of wavenumbers. These quadrature rules are hereafter called "Flat Wave" quadrature and "Gaussian Wave" quadrature, respectively.

In a direct comparison of these rules' ability to integrate sinusoidal functions of different wavenumbers on a triangular patch with size of order 1, it can be seen that for low wavenumbers ($k \lesssim \pi$), the Gauss–Legendre rule works best regardless of how many quadrature points are in the rule (Figure 2.1). This is akin to a heavily overdiscretized problem. For high wavenumbers ($k \gtrsim 4\pi$), none of the rules converges for small numbers of quadrature points. As the number of quadrature points in the rule is increased, all three rules tested begin to converge (as measured by where the slope becomes decidedly negative in plots such as Figure 2.2) at about the same number of points, but both types of wave quadratures outpace the Gauss–Legendre rule in reducing error. For intermediate wavenumbers, $\pi \lesssim k \lesssim 4\pi$, There is no rule with a clear advantage, and as the number of quadrature points in the rule is changed, there are often multiple cross-overs between the amount of error in the different rules (Figure 2.3).

In tests scattering off of a sphere, both wave quadrature rules showed improvements in accuracy over Gauss–Legendre quadrature under certain circumstances. For a six–patch sphere of radius λ, the seven–point Flat Wave rule was about one full digit more accurate than Gauss–Legendre across the full 180-degree bistatic sweep (Figure 2.4).

Any relative advantage of the wave quadrature rules over Gauss–Legendre depends strongly on how converged the problem is for the standard method. In circumstances where the problem is not well converged for Gauss–Legendre quadrature, using either of the two wave quadrature rules does not improve the results. Figure 2.5a shows the result for a radius 2λ sphere discretized in a geometrically similar way to the 1λ sphere used above, and Figure 2.5b shows the result for another similar sphere of radius 4λ, by which time there is no distinction between any of the rules tested, and all are clearly not convergent.

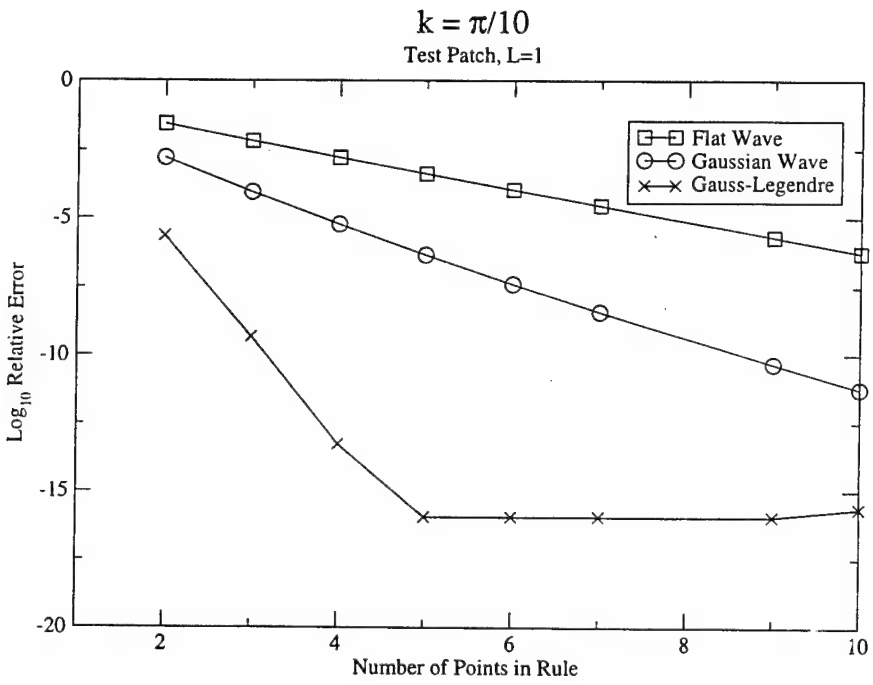

Figure 2.1: $k = \pi/10$. Gauss–Legendre quadrature converges fastest for low wavenumber. This is the regime where the Taylor expansion of the sinusoid is most valid.

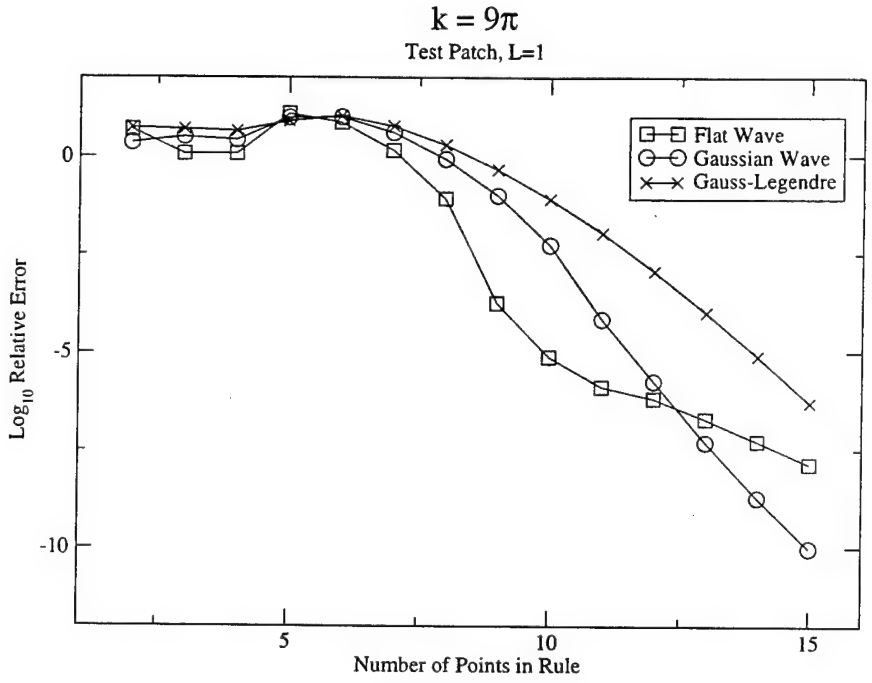

Figure 2.2: $k = 9\pi$. For high wavenumber, both wave quadrature rules surpass Gauss–Legendre, but the Flat Wave rule is superior for more points

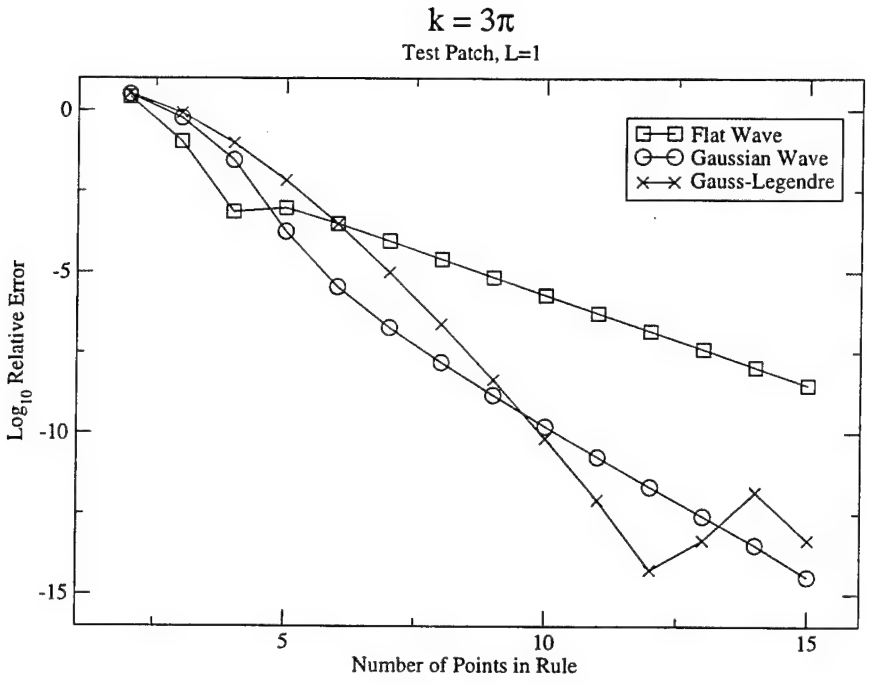

Figure 2.3: $k = 3\pi$. With intermediate wavenumber, there are crossovers between the various quadrature rules.

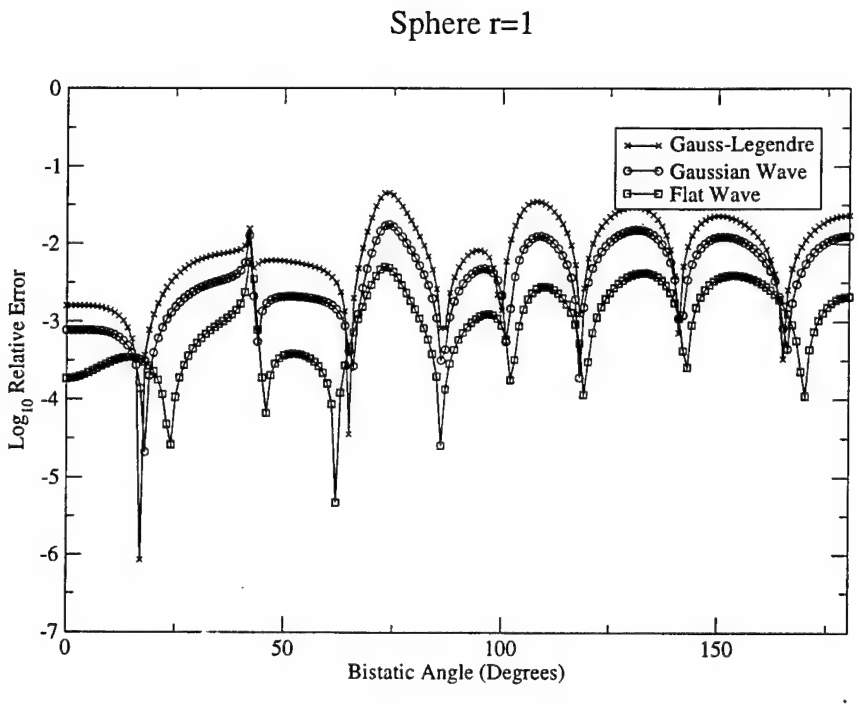

Figure 2.4: Accuracy comparison of three quadrature methods for a sphere of radius λ.

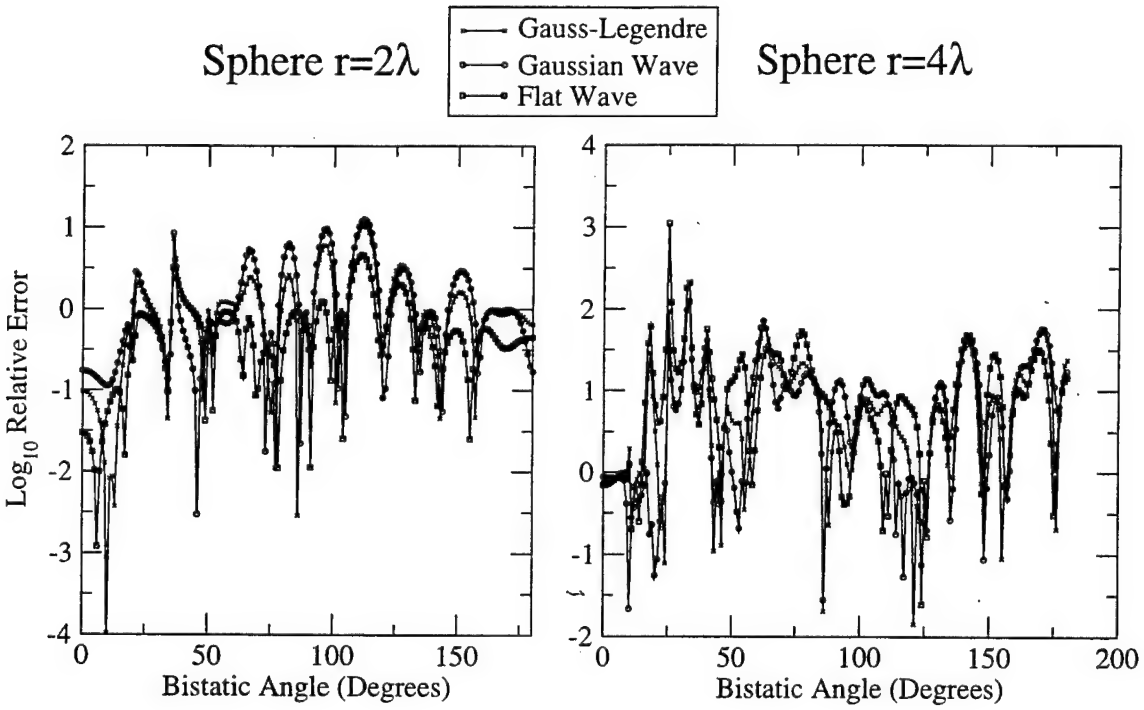

Figure 2.5: In regimes that are poorly converged for Gauss–Legendre quadrature, wave quadrature affords no improvement.

Chapter 3

Low Frequency FMM

We developed a multilevel low frequency sparse FMM operator for the vector Helmholtz kernel which has a theoretical apply time that scales $\mathcal{O}(N)$. It uses a top-down automatic grouping algorithm, which allows the groups to become as small as needed to construct an efficient multilevel operator. This operator is implemented to run on multiprocessor hardware with shared memory and is part of HRL's FastScat scattering code.

points	Dense Time	LF-FMM Time/Scaling	Max Rel Error
960	2.3	1.2	$5 \cdot 10^{-6}$
3840	37	8.5 /1.44	$1 \cdot 10^{-5}$
15360	575	47 /1.23	$1 \cdot 10^{-5}$
61440	9682	226 /1.13	$3 \cdot 10^{-5}$
245760	163432	993/1.07	$2 \cdot 10^{-5}$

Table 3.1: Planar Lattice of Spheres. Apply time in seconds on an Origin 2000 with 400MHz R12000/R12010.

From these data observe the asymptotic approach to the theoretical linear scaling of the multilevel multipole operator. Also note the low overhead cost of the multipole method – the break even point is around one thousand unknowns.

points	Dense Time	LF-FMM Time/Scaling	Max Rel Error
960	2.77	1.14	$8 \cdot 10^{-6}$
3840	44.4	9.74/1.55	$7 \cdot 10^{-6}$
15360	741	58.5/1.29	$6 \cdot 10^{-6}$
61440	12043	452	$3 \cdot 10^{-5}$

Table 3.2: Planar Lattice of Spheres. Apply time/RHS for 4 RHS; seconds on an Origin 200 with 225MHz R10000/R10010.

points	Dense Time	LF-FMM Time	Max Rel Error
480	1	1	$1 \cdot 10^{-15}$
1620	13	5	$1 \cdot 10^{-6}$
3840	71	32	$3 \cdot 10^{-8}$
7500	273	76	$7 \cdot 10^{-7}$
12960	813	102	$2 \cdot 10^{-7}$
20580	2067	254	$9 \cdot 10^{-8}$
30720	4936	576	$5 \cdot 10^{-7}$

Table 3.3: Cubic Lattice. Apply times in seconds on an Origin 2000 with a 400MHz R12000.

3.1 Electromagnetic Multipole Methods for the Helmholtz Equation

The field of a current distribution can be described in the current free region with a multipole expansion. Multipole expansions are often advantageous because complex current distributions can have external fields accurately described with a small number of multipole coefficients. When the size of the source region is large with respect to wavelength the external field needs many moments to describe. In this case, the operator that translates the multipole expansions can be diagonalized.

The Green function for the scalar Helmholtz equation is

$$G(x,y) = \frac{1}{4\pi} \frac{e^{ik|x-y|}}{|x-y|}. \tag{3.1}$$

For $|x| > |y|$ this can be expanded in terms of multipoles as

$$G(x,y) = \frac{ik}{4\pi} \sum_l (-)^l (2l+1)\, P_l(\hat{x}\cdot\hat{y})\, h_l(k|x|)\, j_l(k|y|)\,. \tag{3.2}$$

The dyadic Green function for the electromagnetic equation is

$$G(x,y) = ik\,(1 + \frac{1}{k^2}\nabla\nabla)\,\frac{e^{ik|x-y|}}{4\pi|x-y|}\,. \tag{3.3}$$

Consider two non-intersecting spheres, each with radius R. Sphere X is centered at X and points within the sphere are $X + x$, $|x| < R$. Sphere Y, centered at Y, have points offset from its origin by y.

For a current distribution given by $J(X+x)$ that is zero outside sphere X, the field $E(X+x)$ outside sphere X can be expressed as

$$E(X+x) = \sum_{l=0}^{\infty} \sum_{m=-l}^{l} \alpha_{lm}\, h_l(k|x|)\, Y_{lm}(\Omega(x))\,, \tag{3.4}$$

where the vector coefficients α_{lm} are determined by the current distribution. The unit vector along x is $\hat{x}$. The unit vectors along the cartesian axes are $\bar{x}, \bar{y}, \bar{z}$. The spherical angles are $\cos\theta = \hat{x}\cdot\bar{z}$ and $\cos\phi = \widehat{\zeta}\cdot\bar{x}$, $\zeta = \hat{x} - \bar{z}\cos\theta$. The spherical angles are abbreviated $\Omega = (\cos\theta, \phi)$ and the differential area of the unit sphere is $d\Omega = d\phi \sin\theta d\theta$.

The fields in a source free region are determined by the value of the fields on the boundary. Using the radiation condition at infinity, and the orthogonality of the $Y_{lm}(\Omega)$, the α_{lm} are given by the integration over any shell of radius $A > R$,

$$\alpha_{lm} = h_l^{-1}(kA) \int d\Omega\, Y^*_{lm}(\Omega)\, E(X + x(A,\Omega)) \tag{3.5}$$

The value of A can be arbitrarily large. Letting $A \to \infty$,

$$\alpha_{lm} = i^{l+1}\frac{k}{4\pi} \int d\Omega\, Y^*_{lm}(\Omega) \int d^3x\, e^{-ik(\Omega)\cdot x}\,[1 + \hat{k}(\Omega)\,\hat{k}(\Omega)]\cdot J(X+x)\,. \tag{3.6}$$

In sphere Y, $|y| < R$, free of currents, the field can be expanded as

$$E(Y+y) = \sum_{l=0}^{\infty} \sum_{m=-l}^{l} \beta_{lm}\, j_l(k|y|)\, Y_{lm}(\Omega(y))\,, \tag{3.7}$$

The problem is how to express the β_{lm} in sphere Y in terms of the α_{lm}.

3.2 High Frequency, $kR > 1$

Write the scalar kernel between a point x in sphere X to a point y in sphere Y as,

$$\frac{e^{ik|\delta+\Delta|}}{|\delta+\Delta|} = ik\sum_l (-)^l(2l+1)\; P_l(\hat{\delta}\cdot\hat{\Delta})\; h_l(k|\Delta|)\; j_l(k|\delta|)\,, \tag{3.8}$$

where

$$\delta = x - y,\; \Delta = X - Y,\; |\Delta| > |\delta| \tag{3.9}$$

Using [MF53, Eq. 11.3.47],

$$4\pi i^l\; j_l(k|\delta|)\; P_l(\hat{\delta}\cdot\hat{\Delta}) = \int d\Omega\; e^{ik\hat{r}(\Omega)\cdot\delta}\; P_l(\hat{r}(\Omega)\cdot\hat{\Delta}) \tag{3.10}$$

the Greens function can be written

$$\frac{e^{ik|\delta+\Delta|}}{|\delta+\Delta|} = \frac{ik}{4\pi}\sum_l i^l(2l+1)\; h_l(k|\Delta|)\; \int d\Omega\; e^{ik\hat{r}(\Omega)\cdot\delta}\; P_l(\hat{r}(\Omega)\cdot\hat{\Delta})\,. \tag{3.11}$$

With the truncation of the infinite sum to $L+1$ terms, the sum and integration can be exchanged to define a plane-wave expansion of the Greens function,

$$\frac{e^{ik|\delta+\Delta|}}{|\delta+\Delta|} = \frac{ik}{4\pi}\int d\Omega\; \Gamma_L(\Omega,\Delta)\; e^{ik\hat{r}(\Omega)\cdot\delta}\,, \tag{3.12}$$

where

$$\Gamma_L(\Omega,\Delta) = \sum_l^L i^l(2l+1)\; h_l(k|\Delta|)\; P_l(\hat{r}(\Omega)\cdot\hat{\Delta}) \tag{3.13}$$

Noticing that $\delta < 2R$, an estimate of L comes from the condition that

$$\int_{-1}^{1} dx\; P_l(x)\; e^{2ikxR} < \epsilon\,. \tag{3.14}$$

From this comes the bound, $(k2R)^l/l! < \epsilon$; the l^{th} term in the Taylor series expansion of the exponential is less than ϵ. The empirical formula used in FastScat is

$$L = k2R + \frac{\texttt{digits}}{1.6}\;\ln(k2R+\pi)\,. \tag{3.15}$$

The choice of L establishes that the order of the quadrature rule should be $2L$, or a $Q = (L+1)^2$ point rule with abscissae and weights, $\{\Omega_q, d\Omega_q\}$, given

by a product of a Gauss–Legendre rule in θ and a trapezoidal rule in ϕ. The Green function is expanded in plane waves and is

$$\frac{e^{ik|\delta+\Delta|}}{|\delta+\Delta|} = \frac{ik}{4\pi}\sum_{q}^{Q} d\Omega_q \, e^{ik\hat{r}(\Omega_q)\cdot\delta} \, \Gamma_L(\Omega_q, \Delta)\,. \tag{3.16}$$

3.3 Mid Frequency

Why does the high frequency kernel break as $kR \to 0$? In this limit, the empirical formula for L is $L \approx 0.7$ `digits`.

To get a handle on how many multipole terms are needed, consider the Laplace operator between the two spheres with radius R centered at X and Y with a center to center separation of $6R$. Write the kernel $1/|\delta+\Delta|$. For a δ colinear with Δ this can be written

$$\frac{1}{|\delta+\Delta|} = \frac{1}{6R}\,\frac{1}{1+\delta/6R} = \frac{1}{6R}\,\sum_{l=0}(\frac{-\delta}{6R})^l. \tag{3.17}$$

This is valid because $|\delta| < 2R$. For this expansion to have an error of ϵ for the largest value of δ, L must satisfy the condition

$$(\frac{2}{6})^L < \epsilon\,, \tag{3.18}$$

or

$$L = -\log_3 \epsilon \tag{3.19}$$

which is, approximately, $L = 2$ `digits`.

Using this value for L, the high frequency method can still be used if $k|\Delta|$ is not too small. For such values the leading term in the expansion of $y_l(k|\Delta|)$ is

$$y_l(k|\Delta|) = -\frac{(2l-1)!!}{(k|\Delta|)^{l+1}}. \tag{3.20}$$

It is possible to preserve numerical significance in the sum used to compute $\Gamma_L(\Omega, \Delta)$ if the condition

$$k|\Delta| \geq \sqrt[L]{\frac{(2L-1)!!}{\epsilon\ 10^{15}}} \tag{3.21}$$

holds true, for a floating point precision of 10^{-15}.

The mid frequency method in FastScat uses the high frequency method with this modified value of L and the restriction on the minimum value of $k|\Delta|$. This method has to be used very carefully because it fails catastrophically as $k|\Delta|$ goes to zero.

3.4 Low Frequency

The operator that shifts the α_{pq} of sphere X to the β_{lm} of sphere Y can be determined by evaluation of the fields from the sources in sphere X on a shell of non-zero radius around point Y. Thus

$$\beta_{lm} = \Gamma_{lm,pq}\, \alpha_{pq}\,, \tag{3.22}$$

$$\Gamma_{lm,pq} = j_l^{-1}(kB) \int d\Omega\, Y^*_{lm}(\Omega)\, h_p(k\tilde{R})\, Y_{pq}(\tilde{\Omega})\,. \tag{3.23}$$

In this expression, $\tilde{R}$ and $\tilde{\Omega}$ are the distance and angle from point X to a point at Ω on the shell of radius B centered at Y. The radius B must be such that $j_l(kB) \neq 0$. For the low-frequency domain, the choice $B = R/2$ is not unreasonable. Using this shift operator alone a single stage, $O(N \ln N)$, method can be developed.

To implement an $O(N)$ multilevel scheme, the coefficients must be shifted to and from the centers of parent and child groups. A child group is contained in the sphere centered at X of radius R and this child's parent group is centered at $\tilde{X}$ and has a radius of $2R$. The child group is wholly contained within its parent group.

To shift the α_{pq} centered at X to a parent group of radius $2R$ centered at $\tilde{X}$ near enough so that $|X - \tilde{X}| < R$, use

$$\tilde{\alpha}_{lm} = h_l^{-1}(k2R) \int d\Omega\, Y^*_{lm}(\Omega)\, h_p(k\tilde{R})\, Y_{pq}(\tilde{\Omega})\, \alpha_{pq}\,, \tag{3.24}$$

where $\tilde{R}$ and $\tilde{\Omega}$ are the distance and the angle from point X to a sphere of radius $2R$ centered at $\tilde{X}$. To shift the α_{lm} into the plane-wave expansion used in the high frequency expansion, use,

$$E_\infty(\Omega) = \sum \frac{i^{-1-l}}{k}\, \alpha_{lm}\, Y_{lm}(\Omega)\,. \tag{3.25}$$

Trickling down the hierarchy, the β_{lm} are expressed in terms of the plane wave expansion as

$$\beta_{lm} = 4\pi i^l \int d\Omega \, Y^*_{lm}(\Omega) \, E_\infty(\Omega). \tag{3.26}$$

Within the low-frequency domain, the $\tilde{\beta}_{pq}$ are shifted down with

$$\beta_{lm} = j_l^{-1}(kR/2) \int d\Omega \, Y^*_{lm}(\Omega) \, j_p(k\tilde{R}) \, Y_{pq}(\tilde{\Omega}) \, \tilde{\beta}_{pq} \,, \tag{3.27}$$

where $\tilde{R}$ and $\tilde{\Omega}$ are the distance and the angle from the center of the parent group, $\tilde{X}$, to a point at Ω on the child's shell of radius $R/2$ centered at X.

Chapter 4

Automatic Patch Refinement

We developed a method to refine the discretization and have validated the method on a variety of complex geometric objects. For each run of the scattering program the currents are saved to a file. A postproccessing step reads this file and determines which patches have the largest current error, then it subdivides the patches with the largest errors and generates a new geometry file. The jet is defining a suitable measure of current error, and recognizing that a patch can be split in two directions, one of which may be adequate to resolve the current.

On each patch, two components of the surface current are known at u_q, the Q nodes of a quadrature rule, $j_{\mu,q}$; $\mu \in [1,2]$ and $\hat{e}_{\mu,q}$ is the orthogonal tangent basis. The current at point q is

$$j_q = j_{1,q}\hat{e}_1(u_q) + j_{2,q}\hat{e}_2(u_q).$$

A set of scalar functions, $\phi^k(u)$, can be fit to these values, with,

$$j_{\mu,q} = \sum_{k=0}^{K} \phi^k(u_q)\ \tilde{j}_{\mu,k} = \Phi_{qk}\tilde{j}_k.$$

If the number of independent functions equals the number of quadrature points, the system is square. A reduced system of functions can be constructed from the square set by differentiation with respect to the parametric directions.

$$j_{\mu,q} = \sum_{k=0}^{K} \partial_\nu \phi^k(u_q)\ \bar{j}^{\nu}_{\mu,k} = \Delta_{qk}\bar{j}_k.$$

This system of over-determined equations is singular; the coefficients can be found in a least squares sense using singular value decomposition of the matrix Δ and its pseudo-inverse, $\Delta^{\sim 1}$. The array of errors at quadrature points, $u_q, q \in [1 \ldots Q]$ is given by

$$\epsilon_\mu = (1 - \Delta\Delta^{\sim 1}) j_\mu, \ \mu = 1, 2 \,. \tag{4.1}$$

A measure of the error over the entire patch is given by

$$\varepsilon_\mu = \sum_q w_q \epsilon_{\mu,q}, \quad \mu = 1, 2, \tag{4.2}$$

where w_q are the quadrature's weights. For convex scatters, this measure of error corresponds well with the error in the far field. For other convoluted geometries, there is no such simple measure.

If the error ε_μ is larger than a user specified threshold, then the patch is divided into two halves (in parametric space). This leads to the result that a quadrilateral patch could be divided into 2 or 4 sub-patches, or not at all. It is worthwhile to investigate the error at each point in the hope of finding a point more suitable than the parametric center to divide the patch.

If there are multiple computed currents corresponding to different excitations (e.g. resulting from an angle scan), then the error is the RMS error of all the currents. As the code is currently written, there are at least two currents corresponding to the two polarizations of an incident plane wave.

This code has been tested on a variety of geometries, with PEC and penetrable volumes. The example test case summarized in Table 4.1 is a constellation of PEC objects (a sphere, a thin, flat plate, and a flattened torus, in close proximity to each other) with a dipole source a small fraction of a wavelength off the surface.

Pass	Points	Error
1	1464	$4.17 \cdot 10^{-1}$
3	1626	$1.47 \cdot 10^{-1}$
5	2184	$1.02 \cdot 10^{-1}$
7	3138	$6.06 \cdot 10^{-2}$
9	5586	$3.35 \cdot 10^{-2}$
11	8106	$1.73 \cdot 10^{-2}$
13	11994	$7.28 \cdot 10^{-3}$
15	15144	$3.11 \cdot 10^{-3}$

Table 4.1: Convergence of Automatic patch refining algorithm.

Chapter 5

Raytheon Missile Systems Code Validation

A subcontract was awarded to RMSC for validation of the FastScat code against range measurements. Jack Kennedy, an RMSC engineer, performed the work on the subcontract. The appendix of this document contains a complete report of his investigation.

The validation task included construction and RCS range measurement of three metal targets and numerical simulation of the RCS for these targets using three electromagnetic modeling codes.

The targets were chosen to test the ability of the code to make accurate RCS predictions for targets containing geometric features commonly found on real air vehicles. The first target, a cube six inches on a side, was chosen to test the effectiveness of each code in dealing with targets that contain geometric singularities, in this case, edges and corners. When geometric singularities are present they can interrupt the predominant movement of the surface current, producing standing waves and strong radar reflections. They also result in surface current singularities, which pose a modeling challenge. The second target, a trihedral corner reflector with sides of 4, 6, and 12 inches, was chosen to test each code's ability to predict the RCS of a target for which multiple bounce scattering plays a significant role. The RCS of this target is also affected by the presence of numerous edges and corners. The third target is an 8" long by 8" wide wing-like fin. Its surface is mostly smooth except for an acute angle corner along the trailing edge. This target was chosen to test how well each code computes the RCS of a curved target.

Each target was take to the Raytheon Site A outdoor test range in San

Diego, CA where monostatic RCS measurements at multiple aspects and frequencies were obtained. Details of the measurement process can be found in the full report.

The various measurements were compared against computed results from three electromagnetic modeling codes: FastScat, FISC, and Xpatch. For the two targets comprised of flat surfaces, the results computed by FastScat and FISC matched the experimental results well. Both codes were notably superior to Xpatch in terms of RCS accuracy, especially at low frequency. For the curved target, FastScat and FISC were again quite superior to Xpatch. In this case, however, FISC was generally less accurate than FastScat, especially for lower frequencies. The difference can be attributed to the fact that FastScat internally represents a curved surface using curved mesh elements whereas FISC approximates a curved surface using flat mesh elements. For this reason and others, it was generally possible to obtain more accurate results from FastScat in less time than for FISC.

The overall conclusion is that FastScat is a significantly advanced electromagnetic computation tool that generally produces superb RCS predictions for metal targets.

Appendix A

Fastscat Validation, Final Report

This report is supplied as a separate volume.

Bibliography

[AW95] George B. Arfken and Hans J. Weber. *Mathematical Methods for Physicists.* Academic Press, San Diego, fourth edition, 1995.

[MF53] Phillip M. Morse and Hermann Feshbach. *Methods of Theoretical Physics.* McGraw-Hill, New York, 1953.

[WX99] Stephen Wandzura and Hong Xiao. Quadrature rules on triangles in R^2. Technical Report YALEU/DCS/RR-1168, Yale University, Department of Computer Science, January 1999.